

MODELLING OF PILE DRIVING NOISE BY MEANS OF WAVENUMBER INTEGRATION

Tristan Lippert and Stephan Lippert

Institute of Modelling and Computation, Hamburg University of Technology, Germany

tristan.lippert@tuhh.de

A method for the acoustic simulation of pile driving is presented using the wavenumber integration (WI) approach, in combination with a recently suggested array of point sources, to represent the pile. The fundamentals of the WI are briefly discussed, as are the main acoustic characteristics of pile driving. A reference finite element model is set up to demonstrate these main features and is further compared to a literature example, to ensure its validity. Subsequently, the obtained results are compared to the solutions from WI simulations on the same example. The results are found to be in excellent qualitative agreement, therefore the WI technique seems to be very promising with respect to the acoustic long range prediction in pile driving.

INTRODUCTION

The development and deployment of renewable energy sources is one of the major tasks of our days, since the long term shortage of fossil combustion materials becomes more and more obvious, while the global energy demand continues to rise. To meet this challenge the German government has declared the aim to produce 80% of its total energy consumption from sustainable sources in 2050, with offshore wind energy playing a decisive role [1].

However, one of the major drawbacks of this technology is the possible negative effect on marine wild life during construction. With pile driving being the state of the art foundation for most wind farms, pulses with source sound pressure levels (SPLs) of up to 250dB¹ are produced with each hammer strike. This is likely to cause temporary or even permanent threshold shifts (TTS/PTS) for marine mammals, such as the harbor porpoise, who use their sense of hearing as their primary means of orientation and communication [2]. To protect these endangered species, German authorities have decreed threshold values of 160dB for the sound exposure level (SEL) and 190dB for the peak SPL at a distance of 750m from the pile [3]. To comply with these regulations, sound mitigation measures, such as, bubble curtains or cofferdams, need to be applied. For their design a detailed, numerical model of the pile driving process is needed, both for the assessment of the acoustic impact of planned future wind farms, as well as for the apriority optimization of sound insulation measures to minimize offshore testing time and costs.

Furthermore, apart from offshore wind farms, pile driving takes on a key role in most near shore construction activities, as for example the building of bridges, with comparable possible harm to the environment, see for example Stadler and Woodbury [4].

The relatively large dimensions of several kilometers, in combination with the frequency range of interest stretching up to several kilohertz, make a straight forward, discrete modelling, for example by means of the finite element method (FEM) impractical. Therefore a combined approach of a discrete FE-model that models the complex processes near the

pile with a propagation model that efficiently computes results far from the pile under certain simplifications is desirable.

The present paper focuses on the latter subject, with the wavenumber integration (WI) technique as the propagation method. In this work the basic idea of this method illustrated and the implemented algorithms are briefly discussed. A reference FE-model, that is subsequently explained, is set up and qualitatively compared to results from WI simulations and literature values. Finally, a conclusion and an outlook on planned model extensions are given.

WAVENUMBER INTEGRATION

The simulation of sound propagation in the ocean over long distances via discrete methods is limited by the size of the resulting system of equations. Therefore, a number of alternative schemes have been developed, each involving a number of simplifications, such as normal modes, parabolic equation modelling, wavenumber integration, or ray tracing. For an overview and introduction to each of these schemes, see Jensen et al. [5].

In the present work an investigation by wavenumber integration is used, following Schmidt and Tango [6]. Assuming a two-dimensional, rotational symmetric, stratified (i.e. range-independent) model environment, where sources can only exist on a vertical axis through the origin, the Helmholtz equation reduces to

$$\left[\frac{\partial^2}{\partial r^2} + \frac{\partial^2}{\partial z^2} + k^2(z) \right] \phi(r, z) = S_\omega \delta(r) \delta(z - z_s) \quad (1)$$

where k is the medium wavenumber, ϕ is the potential to be solved for, S_ω is the source strength, $\delta(x)$ is the Dirac function, and z_s is the source depth. The solution of equation (1) can be decomposed into conical wavefronts around the z -axis by means of the forward Hankel transform, from the transform pair

$$f(r, z) = \int_0^\infty F(k_r, z) J_0(k_r r) k_r dk_r \quad (2a)$$

$$F(k_r, z) = \int_0^\infty f(r, z) J_0(k_r r) r dr \quad (2b)$$

¹All dB values are referenced to 1 μ Pascal.

where k_r is the horizontal wavenumber, which can be interpreted as the factor, that determines the inclination of each conical wavefront. The Bessel function J_0 can be expressed by the two Hankel functions $H_0^{1,2}$ by the relation $J_0 = \frac{1}{2} [H_0^1 + H_0^2]$, i.e. identically inclined cones that travel in opposite directions. Thus, the so called depth-separated wave equation is obtained by

$$\left[\frac{\partial^2}{\partial z^2} + (k^2 - k_r^2) \right] \phi(k_r, z) = \frac{S_\omega}{2\pi} \delta(z - z_s) \quad (3)$$

Assuming a purely fluid stratification for a layered waveguide, the solution of equation (3) in each layer m , consists of a particular solution $\hat{\phi}_m$, if a source is present in the layer, and the homogeneous solution of an upward and a downward travelling wave ϕ_m^+ and ϕ_m^- , yielding

$$\phi_m(k_r, z) = \hat{\phi}_m(k_r, z) + A_m^+(k_r) \phi_m^+(k_r, z) + A_m^-(k_r) \phi_m^-(k_r, z) \quad (4)$$

The $2m$ unknown coefficients $A_m^{+,-}$ have to be determined over the $2(m-1)$ continuity conditions for the vertical displacement and the pressure at the $(m-1)$ interfaces between the layers and two boundary conditions, for example a pressure release boundary at the air water interface and an infinite halfspace for the bottom. Analytical solutions for all unknown amplitudes can be found for layers with constant or quadratically varying sound speed profiles, see for example Schmidt [7].

The so-called depth-dependent Green's function $g(k_r, z)$ between a source and a receiver can subsequently be obtained by converting the potential $\phi_m(k_r, z)$ to the physical quantity of interest (e.g. the vertical displacement is defined as $w = \frac{\partial \phi}{\partial z}$). To compute the resulting wave field, $g(k_r, z)$ has to be transformed back from the wavenumber domain to the frequency domain, by means of the backward Hankel transformation, which is given in equation (2).

To automatically obtain frequency results by means of the wavenumber integration approach, e.g. to implement it numerically, some alterations to the described procedure are needed. At first, the infinite integration limit in equation (2) has to be replaced by a finite maximum value $k_{r,max}$ and a horizontal wavenumber discretization Δk_r has to be chosen. Hence, it is crucial to choose $k_{r,max}$ large enough to account for all values of $g(k_r, z)$ that have a meaningful contribution to the integral and to ensure that the wavenumber resolution Δk_r is high enough to avoid aliasing and wrap-around effects in the transformation. For further treatment of numerical transformation requirements, see for example Oppenheim and Schaffer [8].

In the present model, the depth-separated Helmholtz equation (3) is solved by means of the direct global matrix approach suggested by Schmidt and Tango [6]. The algorithm implements an efficient, unconditionally stable solution of the boundary value problem for the pressure p and the displacement w , using an approach resembling finite element discretization of the waveguide in depth. The amplitudes $A_m^{+,-}$ in each layer m are computed for each discrete horizontal wavenumber $k_{r,n}$, with $n = 1 \dots \frac{k_{r,max}}{\Delta k_r}$, what in turn yields the desired, discrete depth-dependent Green's function $g(k_{r,n}, z)$ at all specified receiver depths.

The backward Hankel transformation given in equation (2) is numerically carried out with the help of the so-called fast field approximation (often called fast field program or FFP) suggested by Di Napoli and Deavenport [9]. The approximation is based on the neglect of outgoing waves, i.e. setting the Hankel function $H_0^2 \equiv 0$ in the representation of the Bessel function. Additionally, the remaining Hankel function H_0^1 is replaced by its large argument representation, see for example Abramowitz and Stegun [10]. This yields

$$J_0 = \frac{1}{2} [H_0^1 + H_0^2] \approx \sqrt{\frac{2}{\pi k_r r}} e^{i[k_r r - (m + \frac{1}{2}) \frac{\pi}{2}]} \quad \text{for } k_r r \gg 1 \quad (5)$$

Disregarding the incoming wavefronts is only effecting the wave field close to the source, as is the large argument approximation of $k_r r$ which is already valid for almost all propagation angles at a relatively short distance from the source. The resulting wave field is therefore physically unmeaningful at short ranges r and extremely steep propagation angles, i.e. very small values of k_r . However, steep propagation paths will be damped out rather quickly, due to the multiple reflections at the interfaces and not yield a significant contribution for large values of r and, by definition, the propagation model is used to determine the field at relative large source receiver separations. Hence the use of the fast field approximation is justified in this context.

The main benefit is that the full Hankel transformation, as given in equation (2), reduces to a Fourier transform, as in the FFP representation in equation (5) such that only one exponential function of the argument $k_r r$, multiplied by a constant is left. By doing so, existing, numerically very efficient algorithms can be used for the evaluation of equation (2).

Finally, to better compare the frequency domain results obtained by wavenumber integration with the time domain results from the FE-model, an inverse Fourier transformation is carried out. The convolution of the source signal with the impulse response of the receiver thus reduces to a simple multiplication of the source spectrum S_ω with the Green's function g_ω , and is given by

$$p(r, z, t) = \int_{-\infty}^{\infty} S_\omega g_\omega(r, z) e^{-i\omega t} d\omega \quad (6)$$

For an extensive treatment of time domain transformations and the according requirements see Oppenheim and Schaffer [8].

A tangible illustration of the presented theory of wavenumber integration can be found in figure 1, where it is applied to a simple Pekeris waveguide. As can be seen in figure 1(a), a source is placed in the middle of a fluid layer with a thickness of 100m, which is enclosed by an upper pressure release boundary, i.e. $p(r, z=0) \equiv 0$, and a lower, infinite halfspace of a fluid with higher density and sound speed. In figure 1(b), the solution to equation (4) given by equation (3) is plotted for the receiver depth $z_R = 30$ m for all values of the horizontal wavenumber $k_{r,n}$, at an exemplary frequency of $f = 100$ Hz. Applying the forward Hankel transformation given in equation (2) to this wavenumber spectrum yields the pressure $p(f, r_R, z_R)$. Upon repetition for all frequencies of interest, the frequency response shown in figure 1(c) is

obtained. Convoluting this response with a certain source output signal, here a single sine wavelet, by means of the inverse Fourier transformation given in equation (6), the time series of the receiver $p(t, r_R, z_R)$ is generated. Now the arrival of the direct wave, the first inverse reflection from the pressure release boundary and further reflections can be distinguished, for a full contour plot of the problem see, for example, Lippert et al. [11].

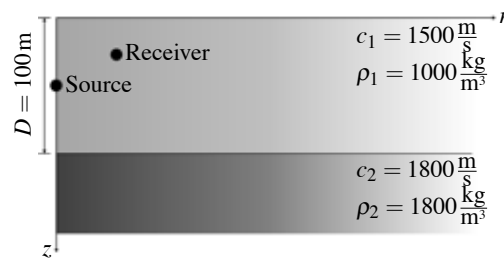
REFERENCE FE-SIMULATION

In this section a basic finite element-model (FE model) is set up to model the acoustics of pile driving. The obtained results are qualitatively compared to an earlier publication of Reinhall and Dahl [12] and used to verify the results obtained with the wavenumber integration.

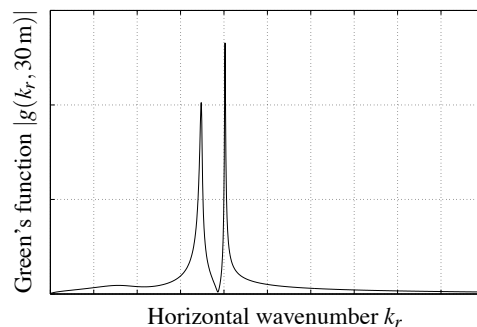
Simplifying, the model is set up as two-dimensional and axis symmetric, assuming a perfectly centered hammer strike. Roughly assuming North Sea offshore conditions, the pile has a total length of 65 m, whereof 20 m are standing in the seafloor, 40 m are surrounded by water, and 5 m protrude from the sea surface. It has a diameter of 3.5 m and a wall thickness of 80 mm. Both the sea bottom and the water column are modeled as fluids, assuming a density of $\rho_w = 1000 \text{ kg/m}^3$ and a sound speed of $c_w = 1450 \text{ m/s}$ for the water phase. The bottom is assumed to be a sandy fluid with a density of $\rho_b = 2034 \text{ kg/m}^3$ and a sound speed of $c_b = 1836 \text{ m/s}$, taken from Hamilton [13]. Additionally, the pile itself is fixed with spring-damper elements, to account for the fact that the vast majority of the strike energy is mechanically absorbed by the intrusion of the pile into the seabed. This somewhat coarse approximation to the real interaction between pile and soil, and the error resulting from it, is accepted, as the results are only to be compared qualitatively. The sea surface is assumed to be a perfect reflector, due to the large difference in impedance between air and water, as is the surface of the protruding part of the pile. The outer boundaries of the model are enclosed by non-reflecting boundary conditions to avoid artificial reflections, thus modelling the surroundings as an infinite layer above an infinite half space. The hammer strike is modelled via a pressure boundary condition. The time-pressure distribution is derived from a simple analytical approach, modelling the pile as a damper with a pile characteristic impedance, acted upon by an accelerated hammer mass, as analytically derived by Deeks and Randolph [14].

The results of three different time steps are depicted in figure 2, where the distinct inclined wavefronts, typical to pile driving can be identified. As shown by Reinhall and Dahl [12] this main contribution of the high sound pressure levels, encountered in acoustic pile driving measurements, can be explained by the occurrence of Mach waves. Typically, Mach waves are associated with jets flying at supersonic speed. Assuming the jet to be an idealized point source, the emitted wavefronts, start to overlap and superimpose each other as the speed of the source is higher than the radiation velocity of the pressure waves (p -waves). The result is a so-called Mach cone, which basically is a high energetic, conical wavefront.

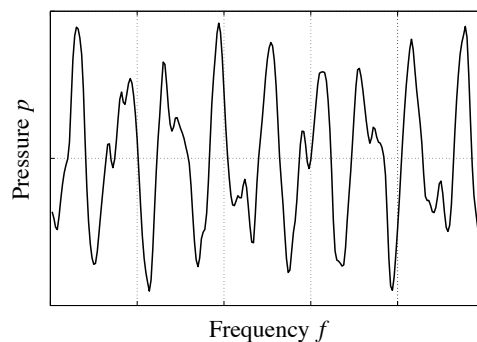
The acoustic radiation from pile driving follows a similar pattern. The hammer strike induces a longitudinal or pressure



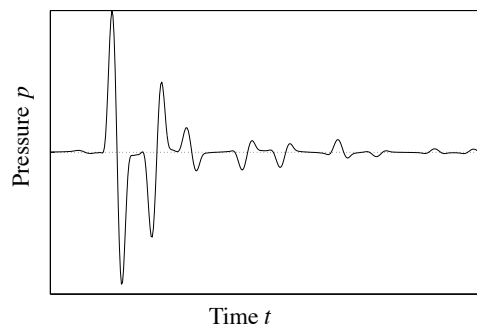
(a) Schematic model sketch (Source: $z_S = 50 \text{ m}$, Receiver: $r_R = 50 \text{ m}$, $z_R = 30 \text{ m}$)



(b) Magnitude of the Green's function at a selected receiver position ($f=100 \text{ Hz}$)



(c) Frequency response at a selected receiver position



(d) Time series at a selected receiver position

Figure 1. Graphic representation of a time series computation with wavenumber integration

wave that travels along down the pile, which in turn triggers a so-called quasi-longitudinal displacement wave. This wave type occurs due to the fact that in solid media, each longitudinal deformation is also coupled to transverse deformation via Poisson's ratio ν , quasi-longitudinal means that the wave is propagating in the longitudinal direction in principle, but with

a transverse component also. In relative slender structures, such as the hollow cylinder regarded here, this transverse deformation component can partly be found to be a surface wave. Additionally, a plate or a rod, for example, have a lower stiffness than an infinite medium consisting of the same material, therefore the propagation speed of an impulse lies below the nominal value, see for example Herbst [15]. As the displacement itself is relatively small, it can be assumed to be a point source. If the pile is simplified as a rod, the propagation velocity of the quasi-longitudinal wave can be determined as $c_{ql} = \sqrt{E/\rho}$, which, depending on the steel used, yields values of approximately $c_{ql} \approx 5000$ m/s. Hence, the analogy to the above mentioned jet example becomes clear, relative to the propagation velocities of the p -waves in the surrounding fluids, the point source is always travelling at supersonic speed, thus producing Mach cones in the same way as described above.

In figure 2, normalized acoustic pressure contours for three exemplary time steps after the hammer impact are depicted. In figure 2(a) the impulse has travelled solely in the water column, developing a clearly identifiable inclined wavefront, e.g. a 2D-slice cut from a Mach cone. The inclination of the wavefront follows directly from the ratio of the propagation velocity of the impulse in the pile c_{ql} and the sound speed in the surrounding fluid c_{fluid} . In this case, the inclination follows as $\phi_w = \arcsin(c_w/c_s) \approx 16$ deg. In figure 2(b) the pulse has passed the interface between the two media and is running in the bottom, the according inclination below the mudline is $\phi_b = \arcsin(c_b/c_s) \approx 20$ deg. The broadening of the resulting wavefront can partly be explained by the higher sound speed c_b in the bottom. In the last figure 2(c) the pulse has reached the lower end of the pile, has been reflected and is now travelling towards the top again. Here one can see that the pressure impulse is subject to a phase shift of 180 deg when it is reflected, due to the drop in impedance between the two media. The less pronounced wavefronts in the bottom are probably partly caused by sound energy leaking from the inner fluid and the inversion of the pulse at the very end of the pile. Additionally imperfections at the nominally non-reflecting boundaries of the model seem to be an issue, as for example discussed by Deeks and Randolph [16].

WAVENUMBER INTEGRATION FOR PILE DRIVING ACOUSTICS

In this section the results produced in the previous section are reproduced with a propagation method, to allow for predictions at large distances from the pile. Based on the exemplified characteristics, Reinhall and Dahl [12] propose a method to model the sound radiation from pile driving by means of a phased point source array. The single contributions from each frequency is determined by means of parabolic equation (PE) modelling. In this contribution, their approach of a point source array is realized with the wavenumber integration technique, described earlier.

The basic idea of the suggested approach is to reproduce the identified Mach waves, by a number of point sources along the pile axis with a fixed spacing. The emitted signal from each of the $n = 1 \dots N$ point sources starts with a time delay of

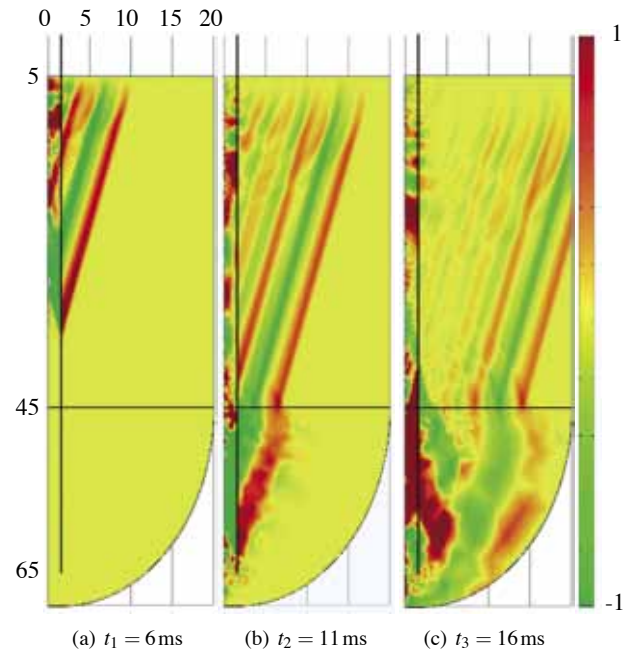


Figure 2. Pressure field contours from the FE model after hammer impact (normalized)

$\Delta t_n = z_{s,n}/c_{ql}$, resulting from the fact that the quasi-longitudinal impulse travels down the pile with a propagation velocity of c_{ql} , which in turn means that at the source position $z_{s,n}$ no signal will be emitted before $t = \Delta t_n$.

The emitted signal from each point source is determined as a single sine wavelet with a frequency of $f_s = 300$ Hz, which is found to be a good approximation for the first wavefront radiated from the pile in the FE simulations. The pile is represented by 13 point sources distributed between the sea surface and the end of the pile, with a spacing of $\Delta z_s = 5$ m. All respective model or material parameters are identical to those described above. The normalized results of the WI simulation are depicted in figure 3.

Before discussion and comparison of the results, some preliminary remarks need to be made. As mentioned above, only the first wavefront is accounted for, hence the noise occurring behind this wavefront cannot be related to the secondary emissions from the FE-results. Also, the region very close to the pile, i.e. the first few metres, are physically unmeaningful, due to the far field approximation discussed earlier. Finally, the relatively wide spacing of the sources leads to somewhat inhomogeneous wavefronts at short distances from the sources, due to the strong curvature. But as the WI is generally used to evaluate the field at some distance from the pile, this problem becomes insignificant, as can be seen from the results. In contrast to its described common application, the WI is subsequently used only in the same range as the FEM to compare the results.

Comparing the simulations, with these reservations, the high consistency of the results becomes obvious. In figure 3(a) the impulse is travelling solely in the water column, while it has reached the end of the pile in figure 3(b). The distinct inclinations of the Mach waves in both media are the same for the FE- and the WI-model, as is the broadening effect of the wavefront in the lower halfspace. In figure 3(c) the impulse has been reflected at the end of the pile and travelling upwards

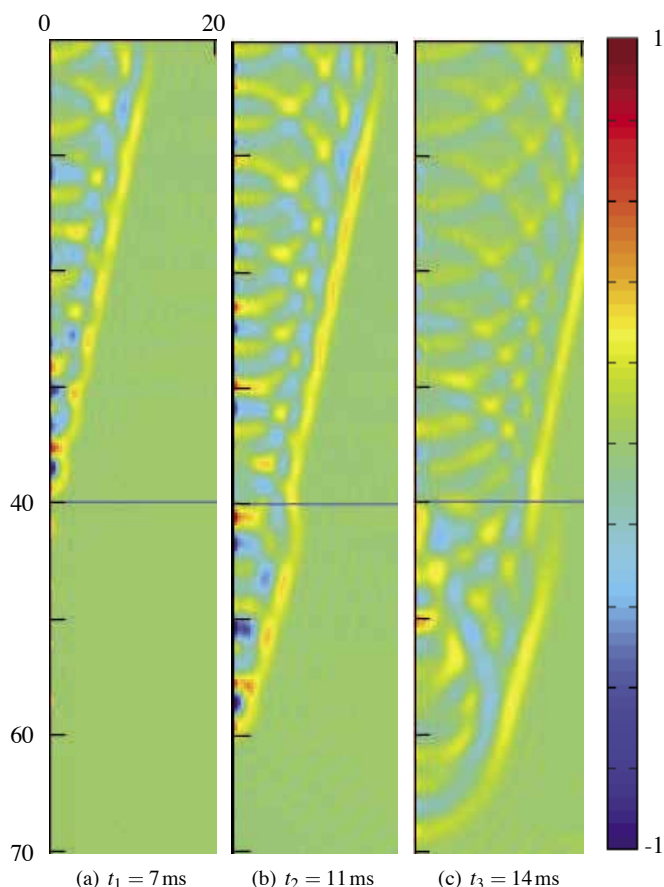


Figure 3. Pressure field contours from the WI-model after hammer impact (normalized)

again, with the expected reversed phase.

It can be seen that developing wavefronts become smooth after approximately 10m. Also, as was the case in the simulations above, the wavefront in the bottom is not as pronounced as it is in the water phase. However, the degree of disfiguration is clearly lower, resulting mainly from the last point source at the pile, which hints to a problem with the non-reflecting boundaries in the FE-model.

Concluding, it can be said that the main characteristics of acoustic pile driving radiation, with the presented WI approach, can be qualitatively reproduced. This could be achieved by means of a relatively simple modelling approach. Therefore, a further enhanced wavenumber integration model is believed to show great promise in the context of acoustic long range predictions of SPLs from pile driving.

CONCLUSIONS AND PROSPECTS

A qualitative modelling of pile driving noise with the help of wavenumber integration is presented and its fundamentals are briefly discussed. To be able to verify the obtained results, an FE model is set up and, first, checked against simulations of Reinhall and Dahl, who identified the main characteristics in pile driving acoustics to be the occurrence of Mach cones. Then, an approach to model the same radiation with the help of parabolic equation modelling, put forward by the same authors, is carried out using wavenumber integration. The qualitative results of the FE and the WI model are compared and found to be in excellent agreement.

As the next step, the comparison of the results on a quantitative basis is planned. After this verification, a validation against extensive planned offshore measurements is envisaged. Therefore, the model is supposed to incorporate both rough boundaries and ambient noise, to account for the actual sea state and weather conditions during the measurements.

ACKNOWLEDGEMENTS

The authors gratefully acknowledge the funding of the BORA project by the Federal Ministry for the Environment, Nature Conservation and Nuclear Safety due to an act of the German Parliament (project ref. no. 0325421 A/B/C). Also, the support of this work by Jonas von Pein is gratefully acknowledged by the authors.

REFERENCES

- [1] Bundesministerium für Umwelt, Naturschutz und Reaktorsicherheit, *Das Energiekonzept der Bundesregierung 2010 und die Energiewende 2011*, 2011
- [2] W.L. Au and M.C. Hastings, *Principles of Marine Bioacoustics*, Springer, Berlin, 2008
- [3] Bundesamt für Seeschifffahrt und Hydrographie, *Leitsätze für die Anwendung der Eingriffsregelung innerhalb der ausschliesslichen Wirtschaftszone*, 2010
- [4] J.H. Stadler and D.P. Woodbury, "Assessing the effects to fishes from pile driving: Application of new hydroacoustic criteria", *Proceedings of Inter-Noise 2009*, Ottawa, Canada, 26-29 August 2009
- [5] F.B. Jensen, W.A. Kuperman, M.B. Porter and H. Schmidt, *Computational Ocean Acoustics*, 2nd edition, Springer, New York, 2011
- [6] H. Schmidt and G. Tango, "Efficient global matrix approach to the computation of synthetic seismograms", *Geophysical Journal of the Royal Astronomical Society* **84**, 331-359 (1986)
- [7] H. Schmidt, *Safari: Seismo-acoustic fast field algorithm for range-independent environments. User's guide*, SACLANTCEN Report no. SR113, Italy, 1988
- [8] A.V. Oppenheim and R.W. Schaffer, *Discrete-time signal processing*, Prentice Hall, 2007
- [9] F.R. Di Napoli and R.L. Deavenport, "Theoretical and numerical Green's function field solution in a plane multilayered medium", *Journal of the Acoustical Society of America* **67**, 92-105 (1980)
- [10] M. Abramowitz and I.A. Stegun, *Pocketbook of mathematical functions*, Verlag Harri Deutsch, Frankfurt, 1984
- [11] T. Lippert, S. Lippert, O. von Estorff, M. Milatz and K. Reimann, "Prediction of pile driving induced underwater noise", *Proceedings of the 19th International Congress on Sound and Vibration*, Vilnius, Lithuania, 8-12 July 2012
- [12] P.G. Reinhall and P.H. Dahl, "Underwater Mach wave radiation from impact pile driving: Theory and observation", *Journal of the Acoustical Society of America* **130**, 1209-1216 (2011)
- [13] E.L. Hamilton, "Geoacoustic modelling of the seafloor", *Journal of the Acoustical Society of America* **68**, 1313-1340 (1980)
- [14] A.J. Deeks and M.F. Randolph, "A simple model for inelastic footing response to transient loading", *International Journal for Numerical and Analytical Methods in Geomechanics* **19**, 307-329 (1995)
- [15] J. Herbst, *Zerstörungsfreie Prüfung von Abwasserkanälen mit Klopferschall*, PhD Thesis, Department of Mechanical Engineering, University of Karlsruhe, 2004
- [16] A.J. Deeks and M.F. Randolph, "Axisymmetric time-domain transmitting boundaries", *Journal of Engineering Mechanics* **120**, 25-42 (1994)